Pulsed iceberg delivery driven by Sturtian ice sheet dynamics

Le Heron, Daniel P.; Busfield, Marie E.

Published in:
Sedimentology

DOI:
10.1111/sed.12225

Publication date:
2016

Citation for published version (APA):
Le Heron, D. P., & Busfield, M. E. (2016). Pulsed iceberg delivery driven by Sturtian ice sheet dynamics: An example from Death Valley, California. *Sedimentology*, *63*(2), 331-349. https://doi.org/10.1111/sed.12225

Pulsed iceberg delivery driven by Sturtian ice sheet dynamics: an example from Death Valley, California

DANIEL P. LE HERON & MARIE E. BUSFIELD

Department of Earth Sciences, Royal Holloway University of London, Egham, Surrey, TW20 0EX (e-mail: daniel.le-heron@rhul.ac.uk)

ABSTRACT

The Kingston Peak Formation is a Cryogenian sedimentary succession that crops out in the Death Valley area, California. It is widely accepted to record pre-glacial conditions (KP1), followed by two glaciations of pan-global extent, the older Sturtian (KP2-3) and younger Marinoan glaciation (KP4). In the type area (the Kingston Range), detailed facies analysis of the Sturtian succession reveals a basal diamictite unit and an upper boulder conglomerate were deposited by proglacial subaqueous sediment gravity flows. An olistostrome unit punctuating the succession is interpreted to result from tectonically-induced downslope mobilisation during isostatic rebound, triggered by significant ice-meltback. Focussing on strata onlapping the olistostrome, this paper provides insight into the processes of glacial re-advance following an intra-Sturtian glacial minimum. The first 50 m of strata above the olistostrome are thinly-bedded turbidites that are devoid of lonestones. A trend toward thicker graded beds upsection, in concert with the gradual appearance and then abundance of lonestones, testifies to the influence of ice rafting and to the resumption of a direct ice sheet influence upon sedimentation. Stratigraphic organisation into thickening and coarsening upward bedsets over a multi-metre scale reveals a subaqueous gravity flow-dominated succession composed of a spectrum of high to low density turbidites, with thick graded boulder-conglomerates at intervals. The finer-grained facies assemblage is heterolithic: current ripple cross-laminated sandstones intercalated with shales that bear delicate granule to pebble-sized dropstones in abundance. Intervals of dropstone-bearing and dropstone-free strata are attributable to dynamic oscillation of the ice margin in the hinterland. Integrating palaeocurrent data with observations from neighbouring outcrop belts allow a detailed palaeogeographic map of the eastern Death Valley area to be compiled for the first time.

INTRODUCTION

The Sturtian glaciation is the oldest of two major glacial intervals in the Cryogenian interval and considered to span approximately 60 Ma (Rooney et al., 2014). In the Death Valley area, California, lower to middle levels of the Kingston Peak Formation are renowned as an excellent example of the interplay between extensional tectonics and glaciation (e.g. Basse, 1978; Miller, 1985; Link et al., 1993; Prave, 1999; Macdonald et al., 2013; Le Heron et al., 2014), contributing to the debate on tectonic versus glaciogenic controls upon diamictites in the Neoproterozoic on a global scale (Eyles and Januszczak, 2004). These deposits, of interpreted Sturtian age (Prave, 1999) have thus received a resurgence of interest since the early sedimentological models were developed (Basse, 1978; Miller, 1985), stemming ultimately from the interest stirred by the snowball Earth hypothesis (Hoffman et al., 1998). Neoproterozoic strata crop out in typically well-exposed but disconnected outcrop belts, providing detailed insight into ice sheet dynamics in the southern Cordillera. Understanding palaeo-ice sheet behaviour, via a detailed scrutiny of facies and stratigraphic architecture, provides valuable boundary conditions for climate models in the Sturtian icehouse world (Hyde et al., 2000; Pierrehumbert, 2005; Le Hir et al., 2007; Pierrehumbert et al., 2011).

In eastern California, the Kingston Peak Formation (**Fig. 1**) preserves an exceptionally well exposed, thick, and laterally extensive succession that includes glaciogenic strata of both early Cryogenian (Sturtian) and late Cryogenian (Marinoan) age (Macdonald et al., 2013; Le Heron et al., 2014). This region, representing the type area of the Kingston Peak Formation, demonstrates clear evidence for a glacial influence on sedimentation (e.g. Mrofka & Kennedy, 2011; Macdonald et al., 2013), including major advance-retreat cycles (Le Heron et al., 2014). In the northern Kingston Range, both Macdonald et al. (2013) and Le Heron et al. (2014) described a >1 km thick olistostrome unit punctuating the Sturtian succession. This interval has been interpreted as a glacial minimum (Le Heron et al., 2014), with retreat of the ice front triggering isostatic rebound, tectonism, and unbuttressing of the carbonate bedrock. These processes led to remobilisation of angular olistoliths downslope, accompanied by background ice-rafting following widespread ice sheet disintegration. Above this horizon, conglomerate and graded sandstone facies are interpreted to record subaqueous outwash during a glacial re-advance (Le Heron et al., 2014). However, the contact between the olistostrome unit and overlying strata is largely obscure in the northern Kingston Range owing to the high proportion of muddy deposits that are typically recessive on hillsides.

This paper targets the southern Kingston Range (**Fig. 1**), where outstanding gulley sections permit the olistostrome and supra-olistostrome units to be clearly distinguished. In contrast to other regions in the Death Valley area, mudstone-rich intervals are well exposed, and demonstrate clear variations in the content of ice-rafted debris. The paper therefore aims to: (1) document the facies associations preserved in the supra-olistostrome unit, (2) comment on the distribution of ice-rafted debris (IRD) in the succession and its relation to ice sheet dynamics and (3) assess the regional palaeogeography during deposition of part of the Kingston Peak Formation, as a first step toward constraining the geometry of the palaeo-ice margin.

REGIONAL GEOLOGY AND STRATIGRAPHY

In ascending order, the Pahrump Group traditionally comprises three subdivisions: the Crystal Spring Formation, the Beck Spring dolomite, and the Kingston Peak Formation (Prave, 1999; Macdonald et al., 2013). Recent detrital zircon ages constrain the upper Crystal Spring Member to younger than 787 ± 11 Ma, which Mahon et al. (2014a) use to propose a separate 'Horse Thief Springs Formation'. This offers a maximum depositional age for the Kingston Peak Formation, which is recognised as older than 635 Ma based upon angular truncation beneath the Noonday Dolomite (Petterson et al., 2011; Macdonald et al., 2013). No palaeomagnetic data are available from the Kingston Peak Formation itself, although Evans (2000) obtained a near-equatorial (01 ± 4º) palaeolatitude from the Johnnie Formation some hundreds of metres stratigraphically upsection.

The Kingston Peak Formation is considered to span two intracratonic rifting events, associated with break-up of the supercontinent Rodinia (Prave, 1999; Mahon et al., 2014a). In the southern Panamint Range, MORB-type pillow lavas are intercalated with diamictites belonging to the lower part of the Kingston Peak Formation in Surprise Canyon (Labotka et al., 1980; Miller, 1985). This key finding, taken together with evidence for "buried faults" led Prave (1999) to propose an early phase of rifting at about 700 Ma. In the Kingston Range, in the vicinity of Horsethief Spring, a series of spectacular en echelon normal faults, dissecting the upper part of the Kingston Peak Formation can be observed on satellite imagery (Le Heron, 2015).

A second phase of rifting during Kingston Peak times was proposed by Prave (1999) at about 600 Ma on account of an olistostrome mapped in Goler Wash, southern Panamint Range. This olistostrome, it was shown, progressively truncated underlying KPF strata down to crystalline basement, and was itself capped by an upper diamictite termed the Wildrose Diamictite (Miller, 1985). Elsewhere in the Death Valley area, olistostromes with km-scale blocks occur in the central and southern Kingston Range (Macdonald et al., 2013; Le Heron et al., 2014 & this paper). Large, angular blocks of dolostone derived from the Crystal Spring Formation are mappable in the Silurian Hills (Kupfer, 1960) where crystalline basement fragments are also common (Basse, 1978).

Evidence for olistostromes in the Pahrump Group is confined to the Kingston Peak Formation. However, it is noted that arkosic sandstone and granular conglomerates- presumably implying downcutting to crystalline basement- occur at intervals in other units, notably in the Crystal Spring Formation (Macdonald et al., 2013). Carbonate conglomerate intervals at the base of the Horse Thief Spring Formation record deposition following a 300 Ma duration hiatus (Mahon et al., 2014a). Regional zircon data suggest an evolution in sediment routing systems, with provenance from the NE (Colorado) during latest Tonian and early Cryogenian time, with progressive input from the SE and E into the Cryogenian (Mahon et al., 2014b).

Macdonald et al. (2013) adopted and refined the regional allostratigraphy for the Cryogenian Kingston Peak Formation developed by Prave (1999). In that framework, the formation is subdivided into 4 units; KP1-4 in ascending stratigraphic order. Owing to the lack of glacial indicators in the lower part of the formation, KP1 is considered to predate the growth of ice sheets that deposited glaciogenic strata of KP2-4. In the Panamint Range, an angular unconformity and package of non-glacial carbonate separates units KP3 and KP4, leading to their interpretation as products of the older Sturtian and younger Marinoan glaciation, respectively (Prave, 1999; Petterson et al., 2011). Le Heron et al. (2014) did not find clear evidence for a KP4 unit in their study area in the northern Kingston Range, although a detailed sedimentary model for units KP2-KP3 was developed in that paper. KP2 consisted entirely of a dropstone-bearing diamictic unit, but the olistostrome and supra-olistostrome succession were restricted to unit KP3 (Le Heron et al., 2014).

THE SOUTHERN KINGSTON RANGE

High quality exposure of unit KP3 is recorded within a series of N-S oriented gulleys that dissect the southern Kingston Range, providing the basis for both correlation (**Fig. 2**) and high resolution facies analysis (**Fig. 3**) that underpin this paper. The contact between the olistostrome and supra-olistostrome succession is well preserved and is sharply defined in the field by a colour change from dark grey weathering, manganiferous deposits to light brown strata (**Fig. 4A**). At the outcrop scale, the olistostrome succession bears very angular blocks of dolostone of boulder size (**Fig. 4B**), extending to km-scale blocks in the northern Kingston Range (Le Heron et al., 2014). This unit is succeeded by heterolithic facies of the supra-olistostrome succession (**Fig. 4C**).

Five detailed sedimentary logs in this area, supplemented by additional data from the northern Kingston Range, are presented herein. The location of logged sections is shown on the geological map (**Fig. 1**). A correlation panel for the strata (**Fig. 2**) clearly demonstrates that some beds can readily be traced (by carefully walking out the contacts in the field), but in other cases, internal complexity is such that bed-by-bed correlation is sometimes impossible. The logged sections are partly simplified, thus an expanded, maximum-detail log is presented for the most important and continuous section (Log 2, **Fig. 3**). For ease of comparison, the facies scheme developed for the northern Kingston Range (Le Heron et al., 2014) and Sperry Wash (Busfield & Le Heron, 2015, this volume) will be adopted herein. Focussing on the topmost unit in the succession (KP3), this study is restricted to three facies associations: 1) Pebble to boulder conglomerate, 2) Interbedded heterolithics, and 3) Lonestone-bearing. This locality is down palaeo-dip from the northern Kingston Range sections, evidenced in measured palaeocurrent orientations, and is further reflected in downslope changes in facies character, discussed below.

Pebble to boulder conglomerate facies association

Description

On the basis of grain size and matrix content, several subfacies are distinguished, namely clast-supported cobble- to boulder-rich conglomerates, clast-supported granule- to pebble-rich conglomerates, and matrix-supported conglomerates (**Fig. 2-3**). Clasts are dominated by carbonates of the Crystal Spring and Beck Spring Dolomite, although sandstone intraclasts are also recognised, and are typically sub-rounded to rounded. Where discoid clasts are present, imbrication is developed in boulders at the base of beds. Stacked conglomeratic bedsets which thicken upwards occur at intervals (e.g. 70 m, 80 m, 95 m, Log 1, **Fig. 2**,).

Continuous intervals of cobble- to boulder-rich conglomerates extend up to 11 m in thickness (e.g. **Fig. 2**, log 1, 57-68 m), but typically occur in beds 1-2 m thick (multiple intervals in log 2, **Figs 2-3; Fig. 4 D**). These facies are predominantly normally-graded, with sharp bed bases in all cases. Some deposits occur above irregular basal contacts, defining lenticular lithosomes 5 m wide and 0.75 m in thickness (**Fig. 4D**). Granule- to pebble-rich conglomerates share many of these characteristics with their coarser-grained counterparts, but tend to occur as thinner (~0.5 m beds). Furthermore, although the cobble- to boulder-rich conglomerates are rare, the granule- to pebble-rich varieties occur with greater regularity, and over intervals of ≤5 m.

Matrix-supported conglomerates are comparatively rare, with bed thicknesses typically <30 cm, attaining clast-width in the case of boulder-bearing beds. In contrast to their pebble to boulder-rich counterparts, these conglomerates are ungraded. Internally, pebble-sized mud chips are observed, forming detached rootless folds in some instances (**Fig. 4 E**).

Interpretation

The clast-supported pebble to boulder conglomerates are interpreted as hyperconcentrated flow deposits (massive) and high-density turbidites (normally-graded) (cf. Lowe, 1982; Kneller, 1995; Mulder & Alexander, 2001; Winsemann et al., 2009; Talling et al., 2012). High sediment concentrations within these flows act to dampen turbulence, and thus hinder the development of bedforms (Talling et al., 2012). The transition from massive to normally-graded varieties is interpreted to reflect flow transformation from moderate cohesive strength debris flows to turbidity currents (Hampton, 1972, Tinterri et al., 2003; Amy & Talling, 2006; Talling et al., 2012). In this scenario, dilution and mixing with the overlying water column during downslope remobilisation promotes increased turbulence and sorting, leading to deposition of normally-graded beds. It is noteworthy that within the northern Kingston Range, massive hyperconcentrated flows dominate (Le Heron et al., 2014), whereas downslope in the southern Kingston Range more dilute, turbidites are far better developed.

Thickening-upwards conglomeratic bedsets are interpreted to record the build-up of lobe elements, the constituent ‘building blocks’ of depositional lobes, which in turn stack to form a lobe complex (Prélat et al., 2009; Macdonald et al., 2011). An axis to off-axis position within the lobe complex is favoured by their coarse calibre and occurrence of amalgamated bedsets (Prélat et al., 2009; Prélat & Hodgson, 2013). Stacked conglomeratic lobe elements are commonly overlain by siltstones of the interbedded heterolithics facies association, representing lobe switching/abandonment.

Matrix-supported conglomerates are interpreted as debris flows of a moderate cohesive strength. Pebble-sized mud chips are interpreted as rip-up clasts incorporated from underlying semi-lithified silt-grade sediments. Their chaotic orientation is consistent with transport within a debris flow (Talling et al., 2012). The rarity of these debrites in the succession of the southern Kingston Range is remarkable given that 6 km further north abundant, matrix-supported conglomerates interpreted as glaciogenic debris flows (GDFs) are preserved (Le Heron et al., 2014). This provides further credence that the southern Kingston Range represents a more distal depositional setting. By analogy to Pleistocene glacier-fed deep marine environments, these sediments are interpreted as elongate debrite lobes interfingering with turbidites on the slope and into the basin plain (Escutia et al., 2000; Taylor et al., 2002).

Interbedded heterolithics facies association

Description

This facies association comprises closely interbedded siltstones and thick-bedded, normally-graded sandstones. They occur either as isolated beds punctuating siltstone facies, or as the basal part of coarsening- and thickening-upward cycles that culminate in conglomerates (**Fig. 5A**). The sandstones exhibit classic sole mark structures at their bases, including flute marks and grooves (**Fig. 5B**), and sharp to irregular bed bases (**Fig. 5C**). Composite cross-laminations with climbing geometries are common. Additionally, flame structures occur at the contact between sandstones and underlying siltstones, and convolute bedding locally disrupts or obscures bed contacts. The graded sandstones occur with similar stratigraphic regularity to their granule- to pebble-rich conglomerate counterparts. Two isolated examples of ungraded sandstones with dune-scale cross-stratification are also recorded, at 25 m and 27 m in Log 1 (**Fig. 2**). The beds are sharp-based and bounded by siltstone facies.

Lonestone-free siltstones constitute approximately 40% of the succession by volume studied in the southern Kingston Range. Intervals of thin-bedded and normally-graded sandstones (2-10 cm thick) are intercalated with siltstone facies. Siltstone-dominated intervals contain variable thicknesses of associated fine- to very fine-grained cross-laminated sandstones. These are expressed as both laterally continuous sets and as laterally disconnected to isolated lenses (**Figs. 5E, F**). Both morphologies exhibit principal palaeoflow towards the SE. In vertical section, both cross-lamina co-sets and stratigraphically isolated cross-lamina intervals occur. Some co-sets express climbing ripple cross-stratification (**Fig. 5E**). Piled load casts occur between superposed laminae, and flame structures occur at the base of some of the thin sandstone intervals (**Fig. 5E**). Detached elliptical load-casts, composed of individual cross-lamina lenses, are also preserved (**Fig. 5F**).

Interpretation

The majority of the thick-bedded sandstones are interpreted as T_A, T_{B-2} and T_C turbidites. The exception may be the cross-stratified sandstones, since the generation of dune-scale cross-stratification is rare in turbidites, possibly owing to the rapidity of sediment fallout suppressing their development (Talling et al., 2012 and refs therein). They are therefore more likely to originate through localised bottom-current reworking than from a primarily turbulent process.

Within the dominant turbidite facies, the contact between T_{B-2} and T_C subdivisions is characterised by a grain size break, recently summarised by Talling et al. (2012) as a commonplace phenomenon in high density turbidites. However, ripple cross-laminated intervals support fully turbulent conditions within low-density turbidity currents (T_C; Mulder & Alexander, 2001; Baas et al., 2011; Talling et al., 2012). Cross-lamination with climbing geometries also reflect fully turbulent conditions but under more rapid rates of sedimentation (Baas, 2000; Kane & Hodgson, 2010; Jobe et al., 2012). The grain size break between T_{B-2} and T_C subdivisions therefore probably records a bipartite structure to the flow in which comparatively higher and lower sediment concentration layers become differentiated as the flow evolves (Mutti, 1992; Mutti et al., 2003). Cross-laminated intervals are bounded by planar laminated and massive siltstones, interpreted to record dilute, low-density turbidity current deposits (T_D and T_{E-1}; Talling et al., 2012), and hemipelagic fallout from the turbulent suspension during waning flow (e.g. Allen et al., 2004). The range of ripple morphologies – both as laterally continuous sets and isolated lenses – indicates fluctuations in sand supply in the dilute turbidity currents, alongside elevated tractional re-working (e.g. Talling et al., 2007, 2012). The piled load casts, detached elliptical load casts and flame structures originate through density contrasts between rapidly deposited sand and underlying muds (Rayleigh-Taylor instabilities; Allen, 1984). The thick, uninterrupted accumulations of this facies over tens of metres are suggestive of continuous input of dilute sediment into the basin.

Lonestone-bearing facies association

Description

Lonestone-bearing strata constitute approximately 30% of the studied sections. Lithologically the sediments are nearly identical to the lonestone-free siltstones of the interbedded heterolithic facies association, comprising massive, laminated and ripple-cross laminated siltstones and fine sandstones. Strata assigned to this facies association tend to exhibit lonestones over dm-scale stratigraphic intervals: note that cm-thick, lonestone-free beds do occur within these intervals. The following considers "outsize clasts" as granule-size and larger were observed, i.e. the assignment was undertaken on the basis of macroscopic rather than microscopic textures.

The lonestone-bearing heterolithics contain granule to boulder-sized lonestones dominated by carbonate (both limestone and dolostone are represented), occasional siltstone and arkose, and rarely quartzite. Clear flexure of underlying laminae beneath these lonestones can be demonstrated (**Figs. 5G-H**). Most commonly, isolated clasts are found in the T_e subdivision, but at some levels, clast clasters are observed. In a large number of cases, puncturing and/or abrupt termination of laminae occurs against the margins of the clast, and non-deformed strata overlie the lonestone.

It should be noted that the size of lonestones varies considerably upsection: the greatest concentration of cobble- and boulder-sized clasts occurs toward the middle part of Log 2 (52-80 m; **Fig. 3**). At this stratigraphic level, it is estimated that pebble- to cobble-grade lonestones account for approximately 8-10% by stratal volume. Lonestone frequency is considerably lower (2-6%) at most other stratigraphic levels. Rarely, concentrated intervals of small lonestones (i.e. granules to small pebbles) occur over 2-3 cm stratigraphic intervals. These thin belts of lonestones transcend clear-cut lithological boundaries in cm-thick graded beds.

In vertical section, four examples of a switch between interbedded heterolithics to the lonestone-bearing facies association are noted in our most complete section (**Fig. 2**). Nevertheless, there are considerable lateral variations on this trend along strike. For example, lonestone-bearing facies in log 2 (27-33 m, **Fig. 2**) correlate with lonestone-free sediments in log 3 (7-10 m, **Fig. 2**). The basal section of Log 1 (**Fig. 2**), which based upon local correlation is not preserved at the base of the other logged sections, demonstrates a notable absence of lonestones.

Interpretation

The lonestone-bearing facies association, akin to comparable lonestone-free siltstones of the interbedded heterolithic facies, are interpreted as the product of fully turbulent, low-density turbidity currents. In this facies association, the deflected and pierced laminae beneath lonestones, in concert with undeformed laminae that drape them, is strong evidence that they are ice-rafted debris (IRD). Bouncing clasts in a turbulent suspension load has long been predicted (Lowe, 1982), but this has not been reproduced experimentally (Talling et al., 2012). Therefore, gravity flow processes should be dismissed as a possibility for forming the dropstone textures. Moreover, dilute, low-density flows would not have the cohesive strength to ‘raft’ up to boulder sized lonestones. Their presence within delicate ripple cross-laminated siltstones and fine sandstones can only readily be explained by ice-rafting processes: other mechanisms for the generation of dropstones (attached to the roots of trees, seaward rafting, animal ingestion: Bennett et al., 1996) are clearly inappropriate for Cryogenian strata.

The lateral and vertical variability of IRD is remarkable. By transcending lithological boundaries, the thin belts of granule- to small pebble-sized lonestones demonstrate that these were also deposited as IRD. Surprisingly, perhaps, no occurrences of “trains” of granule-grade lonestones (i.e. single-clast thick layers of material) are noted in the southern Kingston Range which might point to local winnowing. Correlation between closely spaced sections (**Fig. 2**) suggests that the absence of IRD in small, isolated sections should be treated with caution, underscoring that multiple traverses are important to properly document the trends. Clearly, the absence of IRD in a single section does not imply sedimentation free from glacial influence. The 4 clear transitions from thin bedded heterolithics to lonestone-bearing facies associations observed in the study section imply that IRD delivery to the basin was pulsed.

The potential mechanisms for this are considered in detail elsewhere (Le Heron, 2015). The lateral correlation between lonestone-free and lonestone-bearing deposits may simply imply that certain areas of the Southern Kingston Range escaped the influence of ice-rafted material.

In summary, there appear to be caveats associated with the interpretation of an ice-rafting influence based on lonestones. In addition, the approach does not account for the mudstone fraction, and it has long been known that till pellets can be incorporated into fine-grained rocks, providing more cryptic evidence of IRD. Till pellets are macroscopic, typically rounded, grains of clay or diamicton in modern and Quaternary deposits (Cowan et al., 2012). They have long been thought to form from suspended sediment in interstices between melting ice crystals, developing in a range of supraglacial to subglacial environments (Ovenshine, 1970). The problem is that texturally identical structures are revealed as mudstone aggregates in fluvial settings (Gastaldo et al., 2013) implying that they are not firmly diagnostic of ice-rafting.

Lateral and vertical facies association distributions

The studied sections preserve thick accumulations of thin bedded heterolithics, punctuated at irregular intervals by conglomeratic beds which are typically thicker towards the north-west and thin towards the south-east. The thickest conglomerate package (57-68 m Log 1, **Fig. 2**) can be walked out laterally where it thins to 2 m (4-6 m Log 2, **Fig. 2**). This relationship both demonstrates the extent of along-strike pinch out, and facilitates correlation between other beds.

Upsection, a succession of stacked normally-graded conglomerates (88-102 m Log 1, **Fig. 2**) correlates down-dip with a much more heterogeneous package of thinner conglomerates and sandstones (32.5-59 m Log 2, **Fig. 2**), separated by lonestone-bearing and lonestone-free heterolithics. Similarly, three conglomeratic beds above (117-125 m Log 1, **Fig. 2**) thin over a distance of <100 m between logs 1 and 2, whereas siltstone and fine sandstone packages typically thicken to the SE (**Fig. 2**). This is consistent with the regional trend of successions thickening to the SE observed in the northern Kingston Range (Le Heron et al., 2014), which in tandem with the strongly preferred palaeoflow to the SE (ripple foresets: **Fig. 2**) supports a regional SE-dipping palaeoslope. The pinch out relationships of the coarser facies are therefore interpreted to record proximal to distal thinning as sediment fallout proceeds downslope.

DISCUSSION

Palaeogeography

There is a strong motivation for integrating data from the southern Kingston Range with that from other outcrop belts across the Death Valley area into a regional context. Stratigraphic frameworks have been developed by many other workers, and a detailed facies model has been presented for the Panamint Range toward the west (Miller, 1985). To date, an integrated sedimentological framework for the eastern Death Valley area has not hitherto been proposed. As a first step toward such a model, integrating data from the southern Kingston Range (present paper), the northern and central portions of the range (Le Heron et al., 2014), Sperry Wash (Busfield and Le Heron, 2015, this volume) and the Silurian Hills (Kupfer, 1960; Basse, 1978) allows a gross depositional environments (palaeogeographic) map to be proposed for the south-eastern Death Valley region (**Fig. 7**). This map should be regarded as preliminary. When directional data from the south of the Kingston Range is integrated with the evidence for systematic and consistent thickening from the northern to the southern part of the range (Mrofka, 2010; Macdonald et al., 2013; Le Heron et al., 2014), strong evidence emerges of a regional SE-dipping slope (**Fig. 7**). From this map view, the olistostrome is interpreted to be restricted to a zone south of a NE-SW oriented growth fault system: this is proven in the northern Kingston Range (Prave, 1999; Le Heron et al., 2014) yet speculative north of the Silurian Hills (**Fig. 7**): basement clasts and angular dolostone blocks are mapped in the Kingston Peak Formation in that area (Kupfer, 1960).

Owing to its palaeogeographic position, it is notable that strata in the southern Kingston Range exhibit much more evidence of IRD than their northern counterparts. Toward the northern part of the range, IRD is restricted to strata immediately between the KP2 diamictite and the basal olistostome strata where they occur over a ca 15 m interval (Le Heron et al., 2014). This underscores the importance of palaeogeographic position in the recognition of IRD in Neoproterozoic strata, illustrating that in this case more proximal strata allow a less compelling case for a dropstone influence to be made. In terms of gross facies comparisons, sandy debrites are more commonplace in the northern Kingston Range (Le Heron et al., 2014), whereas high density turbidites are the expression of the coarsest, thickest beds in the interbedded heterolithics in the southern part of the range. This implies that individual glaciogenic debris flow lobes either terminate in an intermediate zone or pass distally into turbidites.

Some 50 km to the west of the southern Kingston Range, the Sperry Wash area is proposed to have periodically occupied an ice-grounding line position, and a generally more proximal position in the basin, during the deposition of unit KP3 (**Fig. 7**) (Busfield and Le Heron, 2015, this volume). When integrated with the evidence for proximal-distal transition from debrites to turbidites in the Kingston Range, it is proposed that the belt dominated by debrite deposition is unlikely to have exceeded more than about 10 km width from proximal to distal at the ice maximum (**Fig. 7**). The Sperry Wash outcrop belt also exhibits evidence for a consistent SE-dipping palaeoslope, with almost identical palaeoflow orientations to the southern Kingston Range (Busfield and Le Heron, 2015, this volume). On our palaeogeographic map, note that we tentatively extend the E-W oriented ice margin to the Saddle Peak Hills, where closely comparable graded beds, IRD-rich intervals, and intrabed deformed zones to the Sperry Wash area can be observed.

Busfield and Le Heron (2015) suggest that the Sperry Wash area may have occupied a fjord setting, hence implying that this part of the basin was fed by a valley glacier draining an upland area to the north. Indeed, Wright et al. (1974) proposed that the area covered by our map was divided into two upland regions during deposition of the Pahrump Group: the Nopah Upland to the north of Sperry Wash and the Kingston Range, and the Mojave Upland range immediately south of the present day Silurian Hills. In addition to the palaeocurrent data herein and contained in Busfield and Le Heron (2015), further evidence for the presence of highlands include the direct contact of the Noonday Dolomite onto gneissose basement at the Gunsight Mine south of Tecopa (Mrofka, 2000).

In the model of Wright et al. (1974), regional slopes from the north and south fed down into an E-W oriented basin (the Armargosa Basin). We adopt this configuration in our preliminary palaeogeography, and propose two ice masses which we term the Mojave ice sheet and the Nopah ice sheet. We also postulate the existence of a spur separating Sperry Wash and Silurian Hills (**Fig. 7**). The reason for this is that whilst lonestones in the Silurian Hills are almost exclusively gneiss, schist and granite (Basse, 1978), none of these lithologies have been observed in the Sperry Wash area, implying the presence of a physical barrier preventing the drift of icebergs toward the north. Conversely, the Sperry Wash area records no evidence for basement clasts akin to those recovered from the Silurian Hills (Busfield and Le Heron, 2015, this volume). Noting that lateral offset between these two areas also certainly occurred during the Cenozoic (Blakely et al. 1999), two credible hypotheses emerge: (1) a silled basin or (2) a ridge of land to prevent the mixing of icebergs, and hence IRD, between them. No data are currently available that allow these hypotheses to be tested.

Further afield, a substantial dataset was collected in the Panamint Range at the western margin of Death Valley in the thesis work of Miller (1983). In the Panamints, the Kingston Peak Formation has historically been divided into a series of members, including the basal Limekiln Spring Member and overlying Surprise Member (Miller, 1985 and refs therein). These rocks, which are overlain by a carbonate unit (Sourdough Limestone Member), were argued to correspond to the first phase of rifting to affect the Death Valley region in the Cryogenian (Prave, 1999), stratigraphically equivalent to units KP2 and KP3 in the Kingston Range (Macdonald et al., 2013) and hence to the Sturtian glacial event. A fence diagram and offlap relationships documented in Miller (1985) suggest a northward-dipping basin margin in that region during this glaciation, including during emplacement of basalts coeval with deposition of the Surprise Member.

Data from the Panamint Range, when considered alongside palaeocurrent data in **Fig. 7**, imply a complex regional basin configuration during deposition of the Sturtian-aged strata. In summary, the data suggest two opposing regional palaeoslopes: a northward slope in the Panamints (Miller, 1985) and in the Silurian Hills (Wright et al., 1974) and a south-eastward slope in the Kingston Range / Sperry Wash area. Although regional rotation during Tertiary transtension cannot be ruled out, , the regional data incorporating observations from the Panamints strengthens the interpretation of two ice masses flowing in opposing directions to the south (the Nopah ice sheet) and to the north (the Mohave ice sheet) (**Fig. 7**).

Global implications

Careful investigation of the Southern Kingston Range succession, together with neighbouring outcrop belts in the Death Valley, illustrates that the strata exhibit strong evidence for glaciomarine sedimentation in a proglacial basin. The predominance of turbidite deposits, with well-expressed SE-directed palaeocurrents, are posited to have evolved from debrites further north in the Kingston Range. Documenting the lateral and vertical distribution of IRD in this region allows us to emphasise that (i) IRD has a complex lateral and vertical distribution on a local scale in proglacial strata but in spite of this (ii) the record of ice rafting is more clearly expressed at a distance of some tens of km from the palaeo-ice margin than in more proximal settings. Our palaeogeographic map based on these data is the first detailed attempt to do so in the eastern Death Valley area. Moreover, it allows a first order interpretation of the location and orientation of the ice grounding zone when integrated from data in Sperry Wash (Busfield and Le Heron, 2015, this volume). It is notable that grounding-line wedges have been documented from other Cryogenian sedimentary records (Domack and Hoffman, 2011), and their recognition is an important step in palaeogeographic reconstruction.

Cryogenian glacial deposits continue to be viewed as deposits of snowball Earth conditions (Hoffman et al., 1998) by much of the geological community, rather than deposits of ice sheets exhibiting a near-identical sedimentary record to their Phanerozoic counterparts (e.g. Etienne et al., 2007). Other interpretations such as a “slushball Earth” compromise including the relative contributions of a high-tilt Earth and tectonic processes (see Fairchild and Kennedy, 2007, for a review) are commonly sidelined. Papers attempting to quantify, via numerical models, the magnitude of postglacial sea-level rise (Creveling and Mitrovica, 2014), to simulate the climate of Cryogenian glaciations (Feulner and Kienert, 2014), or wishing to emphasise the significance of benthic macroscopic phototrophs (fossil finds) in associated strata (Ye et al., 2015) all begin with the starting assumption of a snowball Earth with a global, or near global ice cover. Predictions of the snowball Earth model stipulate equatorial temperatures of −20 °C (Hoffman and Schrag, 2002). However, sedimentological evidence from the Marinoan glacial succession of South Australia reveals periglacial sand wedges demonstrating an active regolith layer at the palaeotropics, and therefore mean surface temperatures “within a few degrees of freezing” (Ewing et al., 2014).

In the Sturtian record, meanwhile, the Kingston Peak Formation does not support the interpretation of a continuous ice cover, with transitions from ice contact to proglacial basins envisaged. In concert with previous studies emphasising IRD abundance in Cryogenian strata (Condon et al., 2002; Leather et al., 2002), or wave generated structures implying ice-free areas (Allen and Etienne, 2008; Busfield and Le Heron, 2014), we envisage highly dynamic, polythermal ice masses (Hambrey and Glasser, 2012). These ice masses exhibited multiple advance and retreat cycles, releasing prodigious volumes of meltwater to explain repeatedly stacked glaciogenic debris flows (in more proximal settings) and turbidites (in more distal settings) in tandem with IRD. These characteristics strongly negate the requirement for refugia or speculative polynyas to support “survivalist” ecosystems (e.g. Ye et al., 2015), particularly as glacial minima conditions (Le Heron et al., 2014) and possible interglacials are expected to yield open water conditions. In summary, the collection of basic sedimentological datasets, to facilitate the compilation of palaeogeographic maps, remains fundamental to the debate.

CONCLUSIONS

- In the southern part of the Kingston Range, a multi-km thick succession of the Kingston Peak Formation includes an olistostrome succession and a supra-olistostrome succession in unit KP3. In the central Kingston Range, the olistostrome was interpreted as the deposits of a Sturtian glacial minimum, produced during an isostatic rebound event prior to glacial re-advance (Le Heron et al., 2014). In the south of the range, exceptional exposure quality allows detailed documentation of the supra-olistostrome deposits via 5 high resolution sedimentary logs;
- The supra-olistostrome succession contains three facies associations. The pebble to boulder conglomerate facies association records deposition from hyperconcentrated flows to high density turbidity flows, ultimately debouched from the ice margin. The heterolithic facies association is the more distal part of this system, deposited by more dilute turbidity currents. The lonestone-bearing facies association, meanwhile, additionally records the accumulation of ice-rafted debris in this underflow-dominated proglacial setting;
- Consideration of the lateral relationship between facies illustrates that although the thickest beds and intervals can be traced at outcrop over several hundreds of metres, significant bed thinning does occur over several tens of metres. Together with palaeocurrent data recovered from ripple cross-lamination, grooves and flutes casts, a pronounced SE-directed slope is identified;
- A preliminary palaeogeographic map of the eastern Death Valley area interprets a consistent SE-directed palaeoslope that included all parts of the Kingston Range and the Sperry Wash area. An ice mass grounded in the latter area released efflux as glaciogenic debris flows into the basin, forming a conglomerate-rich apron about 10 km in extent from proximal to distal. Beyond this zone, turbidite deposition was dominant, and IRD is well preserved.

Acknowledgements: this work was part-supported by the Geological Society of London Fermor Fund. This paper is dedicated to Tony Prave to whom the authors are indebted for his general advice, and discussions in the field in an earlier field season which led to our 2014 paper from an earlier phase of work. We are grateful to the chief editor, Nigel Mountney, for his patience, to three anonymous reviewers, and to Julian Dowdeswell for his thoughts on the manuscript. This led to a much improved paper.

REFERENCES

Allen, J.R.L. (1984) Sedimentary Structures: Their Character and Physical Basis, volumes I and II. Elsevier, Amsterdam.

Allen, P.A. and **Etienne, J.L.** (2008) Sedimentary challenge to snowball Earth. *Nature Geoscience*, **1**, 817–825.

Amy, L. and **Talling, P.J.** (2006) Anatomy of turbidite and debrite sandstones based on long distance (120 x 35 km) bed correlation, Marnoso-arenacea Formation, Northern Apennines, Italy. *Sedimentology*, **53**, 161–212.

Baas, J.H. (2000) Duration of deposition from decelerating high-density turbidity currents. *Sed. Geol*., **136**, 71–88.

Baas, J.H., Best, J.L. and **Peakall, J.** (2011) Depositional processes, bedform development and hybrid flows in rapidly decelerated cohesive (mud-sand) sediment flows. *Sedimentology*, **58**, 1953–1987.

Basse, R.A. (1978) Stratigraphy, Sedimentology and Depositional Setting of the Late Precambrian Pahrump Group, Silurian Hills, California. MS Thesis, Stanford University, 86p.

Bennett, M.R., Doyle, P. and **Mather, A.E.** (1996) Dropstones: their origin and significance. *Palaeogeography Palaeoclimatology Palaeoecology*, **121**, 31–339.

Blakely, R.J., Jachens, R.C., Calzia, J.P. and **Langenheim, V.E.** (1999). Cenozoic basins of the Death Valley extended terrane as reflected in regional-scale gravity anomalies. In: Wright, L.A. & Troxel, B.W. (eds.): Cenozoic Basins of the Death Valley Region. Boulder, Colorado, Geological Society of America Special Paper 333.

Busfield, M.E. and **Le Heron, D.P.** (2014). Sequencing the Sturtian icehouse: dynamic ice behaviour in South Australia. *Journal of the Geological Society of London*, **171**, 443-456.

Busfield, M.E. and **Le Heron, D.P.** (2015, this volume) A Neoproterozoic ice advance sequence, Sperry Wash, California. *Sedimentology***.**

Condon, D.J., Prave, A.R. and **Benn, D.I. 2002.** Neoproterozoic glacial-rainout intervals: Observations and implications. *Geology*, **30**, 35-38.

Cowan, E.A., Christofferson, P. and **Powell, R.D.** (2012) Sedimentological Signature of A Deformable Bed Preserved Beneath An Ice Stream In A Late Pleistocene Glacial Sequence, Ross Sea, Antarctica. *Journal of Sedimentary Research*, **82**, 270–282.

Creveling, J.R. and **Mitrovica, J.X.** (2014) The sea-level fingerprint of a Snowball Earth deglaciation. *Earth and Planetary Science Letters*, **399**, 74-85.

Domack, E.W. and **Hoffman, P.F.** (2011) An ice grounding-line wedge from the Ghaub glaciation (635 Ma) on the distal foreslope of the Otavi carbonate platform, Namibia, and its bearing on the snowball Earth hypothesis. *Geol. Soc. Am. Bull.*, **123**, 1448-1477.

Escutia, C., Eittreim, S.L., Cooper, A.K. and **Nelson, C.H.** (2000) Morphology and acoustic character of the Antarctic Wilkes Land turbidite systems: icesheet- sourced versus river-sourced fans. *Journal of Sedimentary Research*, **70**, 84-93.

Etienne, J.L., Allen, P.A., Rieu, R. and **Le Guerroue, E.** (2007) Neoproterozoic glaciated basins: a critical review of the Snowball Earth hypothesis by comparison with Phanerozoic glaciations, in: Hambrey, M.J., Christoffersen, P., Glasser, N.F., Hubbard, B. (Eds.), Glacial Processes and Products. International Association of Sedimentologists, Special Publications, 436 pp.

Evans, D.A.D. (2000) Stratigraphic, geochronological, and paleomagnetic constraints upon the Neoproterozoic climatic paradox. *American Journal of Science*, **300**, 347-433.

Ewing, R.C., Eisenman, I., Lamb, M.P., Poppick, L., Maloof, A.C. and **Fischer, W.W.** (2014) New constraints on equatorial temperatures during a late Neoproterozoic snowball Earth glaciation. *Earth and Planetary Science Letters*, **406**, 110-122.

Eyles, N. and **Januszczak, N.** (2004) 'Zipper-rift': a tectonic model for Neoproterozoic glaciations during the breakup of Rodinia after 750 Ma. *Earth Science Reviews*, **65**, 1–73.

Fairchild, I.J. and **Kennedy, M.J.** (2007) Neoproterozoic glaciation in the Earth System. *Journal of the Geological Society of London*, **164**, 895–921.

Feulner, G. and **Kienert, H.** (2014) Climate simulations of Neoproterozoic Snowball Earth events; similar critical carbon dioxide levels for the Sturtian and Marinoan glaciations. *Earth and Planetary Science Letters*, **404**, 200-205.

Gastaldo, R.A., Pludow, B.A. and **Neveling, J.** (2013) Mud Aggregates from the Katberg Formation, South Africa: Additional Evidence for Early Triassic Degradational Landscapes. *Journal of Sedimentary Research*, 83, 531-540.

Hambrey, M.J. and **Glasser, N.F.** (2012) Discriminating glacier thermal and dynamic regimes in the sedimentary record**.** *Sedimentary Geology*, **251**, 1-33.

Hampton, M.A. (1972) The role of subaqueous debris flow in generating turbidity currents. *J. Sed. Petrol*., **42**, 775–793.

Hoffman, P.F. and **Schrag, D.P.** (2002) The snowball Earth hypothesis: testing the limits of global change. *Terra Nova*, **14**, 129-155.

Hoffman, P.F., Kaufman, A.J., Halverson, G.P. and **Schrag, D.P.** (1998) A Neoproterozoic Snowball Earth. *Science*, **281**, 1342-1346.

Hyde, W.T., Crowley, T.J., Baum, S.K. and **Peltier, R.** (2000) Neoproterozoic 'snowball Earth' simulations with a coupled climate/ice-sheet model. *Nature*, **405**, 425–429.

Jobe, Z.R., Lowe, D.R. and **Morris, W.R. (2012)** Climbing-ripple successions in turbidite systems: depositional environments, sedimentation rates and accumulation times. *Sedimentology*, **59**, 867–898.

Kane, I.A. and **Hodgson, D.** (2010) Submarine channel levees: criteria for recognition of levee subenvironments: exhumed examples from The Rosario Fm (Baja, Mexico) and the Laingsburg Fm. (Karoo Basin). *Mar. Petrol. Geol*., **28**, 807–823.

Kneller, B. C. (1995) Beyond the turbidite paradigm: physical models for deposition of turbidites and their implications for reservoir potential. *In*: Characterization of Deep Marine Systems (Eds A.J. Hartley and D.J. Prosser), *Geol. Soc. Spec. Publ*., **94**, 31–49.

Kupfer, D.H. (1960) Thrust faulting and chaos structure, Silurian Hills, San Bernadino County, California. *GSA Bulletin*, **71**, 181-214.

Labotka, T.C., Albee, A.L., Lanphere, M.A. and **McDowell, S.D.** (1980) Stratigraphy, structure and metamorphism in the central Panamint Mountains (Telescope Peak quadrangle), Death Valley area, California, *Geological Society of America Bulletin*, **91**, 843–933.

Leather, J., Allen, P.A., Brasier, M.D. and **Cozzi, A.** (2002) Neoproterozoic snowball Earth under scrutiny: Evidence from the Fiq glaciation of Oman. *Geology*, **30**, 891–894.

Link, P.K., Miller, J.M.G. and **Christie-Blick, N.** (1993) Glacial-marine facies in a continental rift environment: Neoproterozoic rocks of the western United States Cordillera. In: Deynoux, M., Miller, J.M.G., Domack, E.W., Eyles, N., Fairchild, I.J., Young, G.M. (Eds.), Earth's Glacial Record. Cambridge Univ. Press, Cambridge, 29– 46.

Le Heron, D.P. (2015) The significance of ice-rafted debris in Sturtian glacial successions. *Sedimentary Geology*, **322**, 19-33.

Le Heron, D.P., Busfield, M.E. and **Prave, A.R.** (2014) Neoproterozoic ice sheets and olistoliths: multiple glacial cycles in the Kingston Peak Formation, California. *Journal of the Geological Society, London*, doi: 10.1144/jgs2013-130

Le Hir, G., Ramstein, G., Donnadieu, Y. and **Pierrehumbert, R.T.** (2007) Investigating plausible mechanisms to trigger a deglaciation from a hard Snowball Earth, *C. R. Geosci*, **339**, 274–287.

Lowe, D.R. (1982) Sediment gravity flows: II. Depositional models with special reference to the deposits of high-density turbidity currents. *J. Sed. Petrol.*, **52**, 279-297.

Macdonald, F.A., Prave, A.R., Petterson, R., Smith, E.F., Pruss, S.B., Oates, K., Trotzuk, D. and **Fallick, A.E.** (2013) The Laurentian record of Neoproterozoic glaciation, tectonism, and eukaryotic evolution in Death Valley, California. *Geological Society of America Bulletin*, doi: 10.1130/B30789.1

Mahon, R.C., Dehler, C.M., Link, P.K., Karlstrom, K.E. and **Gehrels, G.E.** (2014a) geochronologic and stratigraphic constraints on the Mesoproterozoic and Neoproterozoic Pahrump Group, Death Valley, California: A record of the assembly, stability, and breakup of Rodinia. *Geological Society of America Bulletin*, **126**, 652-664.

Mahon, R.C., Dehler, C.M., Link, P.K., Karlstrom, K.E. and **Gehrels, G.E.** (2014b) detrital zircon provenance and paleogeography of the Pahrump Group and overlying strata, Death Valley, California. *Precambrian Research*, **251**, 102-117.

Miller, J.M.G. (1983) Stratigraphy and sedimentology of the upper Proterozoic Kingston Peak Formation, Panamint Range, eastern California. PhD Thesis, Santa Barbara, California, University of California, 335 pp.

Miller, J.M.G. (1985) Glacial and syntectonic sedimentation: The upper Proterozoic Kingston Peak Formation, southern Panamint Range, eastern California. *Geological Society of America Bulletin*, **96,** 1537-1553.

Mrofka, D. (2010) Competing models for the timing of Cryogenian Glaciation: Evidence from the Kingston Peak Formation, southeastern California. PhD dissertation, University of California, Riverside.

Mrofka, D. and **Kennedy, M.** (2011) The Kingston Peak Formation in the eastern Death Valley region. In: *The Geological Record of Neoproterozoic Glaciations* (Eds E. Arnaud, G.P. Halverson and G. Shields-Zhou). Geological Society, London, Memoirs, **36**, 449-458.

Mulder, T. and **Alexander, A.** (2001) The physical character of subaqueous sedimentary density flows and their deposits. *Sedimentology*, **48**, 269–299.

Mutti, E. (1992) Turbidite Sandstones. Istituto di Geologia Universita di Parma & AGIP, San Donato Milanese, 275 pp.

Mutti, E., Tinterri, R., Benevelli, G., diBase, D. and **Cavanna, G.** (2003) Deltaic, mixed and turbidite sedimentation of ancient foreland basins. *Mar. Petrol. Geol.*, **20**, 733–755.

Ovenshine, A.T. (1970) Observations of iceberg rafting in Glacier Bay, Alaska, and the identification of ancient ice-rafted deposits. *Geological Society of America Bulletin*, **81**, 891-894.

Petterson, R., Prave, A.R. and **Wernicke, B.P.** (2011) Glaciogenic and related strata of the Neoproterozoic Kingston Peak Formation in the Panamint Range, Death Valley region, California. In: *The Geological Record of Neoproterozoic Glaciations* (Eds E. Arnaud, G.P. Halverson and G. Shields-Zhou). Geological Society, London, Memoirs, **36**, 449-458.

Pierrehumbert, R.T. (2005) Climate dynamics of a hard snowball Earth. *J. Geophys Res -- Atmospheres*. 110(D1) D01111 doi:10.1029/2004JD005162

Pierrehumbert, R.T., Abbot, D., Voight, A. and **Koll, D. (2011)** Neoproterozoic Climate. *Annual Reviews of Earth and Planetary Sciences*, **39**, 417–60.

Prave, A.R. (1999) Two diamictites, two cap carbonates, two $\delta^{13}C$ excursions, two rifts: the Neoproterozoic Kingston Peak Formation, Death Valley, California. *Geology*, **27**, 339-324.

Prélat, A. and **Hodgson, D.M.** (2013) The full range of turbidite bed thickness patterns in submarine lobes: controls and implications. *Journal of the Geological Society*, **170**, 209-214.

Prélat, A., Covault, J.A., Hodgson, D.M., Fildani, A. and **Flint, S.S.** (2010) Intrinsic controls on the range of volumes, morphologies, and dimensions of submarine lobes. *Sedimentary Geology*, **232**, 66-76.

Rooney, A.D., Macdonald, F.A., Strauss, J.V., Dudás, F. Ö., Hallmann, C. and **Selby, D.** (2014) Re-Os Geochronology and coupled Os-Sr isotope constraints on the Sturtian snowball Earth. *Proceedings of the National Academy of Sciences*, **111**, 51-56.

Talling, P.J., Amy, L.A., Wynn, R.B., Blackbourn, G. and **Gibson, O.** (2007) Turbidity current evolution deduced from extensive thin turbidites: Marnoso-arenacea Formation (Miocene), Italian Apennines. *J. Sed. Res*., **77**, 172–196.

Talling, P.J., Masson, D.G., Sumner, E.J. and **Malgesini, G.** (2012) Subaqueous sediment density flows: Depositional processes and deposit types. *Sedimentology*, **59**, 1937–2003.

Taylor, J., Dowdeswell, J.A., Kenyon, N.H. and **O'Cofaigh, C.** (2002) Late Quaternary architecture of trough-mouth fans: debris flows and suspended sediments on the Norwegian margin. In: *Glacier-Influenced Sedimentation on High-Latitude Continental Margins* (Eds J.A. Dowdeswell and C. O'Cofaigh), *Geol. Soc. London Spec. Publ*., **203**, 55–71.

Tinterri, R, Drago, M., Consomi, A., Davoli, G. and **Mutti, E.** (2003) Modelling subaqeous bipartite sediment gravity flows on the basis of outcrop constraints: first results. *Mar. Pet. Geol*., **20**, 911–933.

Winsemann, J., Hornung, J.J., Meinsen, J., Bußmann, M. and **Weber, C.** (2009) Anatomy of a subaqueous ice-contact fan and delta complex, Middle Pleistocene, North-west Germany. *Sedimentology*, **56**, 1041-1076.

Wright, L.A., Troxel, B.W., Williams, E.G., Roberts, M.T. and **Diehl, P.E.** (1974) Precambrian sedimentary environments of the Death Valley region, eastern California and Nevada. In: *Geological Society of America, Guidebook: Death Valley region, California and Nevada* [prepared for the 70th Annual Meeting of Cordilleran Section, Geological Society of America]. The Death Valley Publishing Company, Shoshone, CA, 27–35.

Ye, Q., Tong, J., Xiao, S., Zhu, S., An, Z., Tian, L. and **Hu, J.** (2015) The survival of benthic macroscopic phototrophs on a Neoproterozoic snowball Earth. *Geology*, **43**, 507-510.

Figure captions

Figure 1. Overview map of the main outcrops of Neoproterozoic strata in Death Valley. B: Satellite image of the southernmost part of the Kingston Range (see A for location). C: Simple geological map of the southern Kingston Range, covering the same geographic area as the satellite image (B). The colour scheme matches that of Le Heron et al. (2014) for comparison with strata further north in the range. Shown on this map are the locations of detailed sedimentary logs which are presented in Figure 2.

Figure 2: Sedimentary logs corresponding to each of the locations that are shown in Fig. 1 C. Note that three facies associations are recognised in this study. Three lines of evidence for a SE-dipping, major palaeoslope can be established: (1), palaeocurrents in the rose diagram, showing regional-dip corrected cross-laminations plus flute casts and grooves; (2), consistent thinning and pinch out of the conglomerates on each of the logs in the same direction; (3),

based on previous evidence (Le Heron et al., 2014), thickening of the entire Kingston Peak Formation away from growth faults in the Horsethief Spring area to the NW. On the logs, note the clear alternation/ differentiation of lonestone-bearing and lonestone-free thin bedded heterolithic deposits.

Figure 3: Expanded version of logged section 2 (Fig. 2) at a higher resolution, without simplification, illustrating the vertical facies transitions at maximum-level detail. This log is a key section owing to almost continuous exposure of the finer-grained fraction in water-washed gullies, enabling the presence and absence of ice-rafted debris (IRD) to be documented to a high level of confidence.

Figure 4: Macroscale phenomena. A: landscape-scale view of the contact between the top of the olistostrome complex in KP3 and the base of the supra-olistostrome succession (see also Fig. 1 C). B: Olistostrome complex at the outcrop scale, with extremely angular blocks of dolostone embedded with a manganese-rich matrix. Kilometre-scale dolostone blocks also occur at intervals (Fig. 1 C). C: View of the basal part of the supra-olistostrome complex, characterised by well stratified interbedded sandstones, conglomerates, and heterolithic strata (documented in Fig. 2, log 1, 0-55 m). D: Typical view of a series of thickly-bedded sandstones (next to geologist in view) sharply overlain by a graded conglomerate bed (124 m, log 1, Fig. 2). E: Top of a thickening-up, coarsening upward interval (87 m log 2; Figs. 2 & 3), culminating in a normally-graded conglomerate unit.

Figure 5: Mesoscale phenomena. A: Flute casts indicating SE flow. B: Classic $T_{A\text{-}C}$ cycle. Note the characteristic sharp grain-size break between the parallel laminated T_B interval and the ripple cross-laminated T_C subdivision. C: Intercalated graded sandstone beds and lonestone-bearing shales (arrowed). D: Climbing ripple sets, starved ripple lenses, and shale laminae. Load clasts occur beneath the sandstone intervals. E: 2 m along strike from image in D, showing a small dolostone granule with classic impact structure (hence a dropstone) beneath. F: Pebble-sized dropstone, clearing puncturing a cm-thick graded bed. G: Boulder-sized dropstone, typical of the interval 55-80 m in log 2. H: Matrix supported, muddy conglomerare with detached, rootless, recumbent fold within the bed. Scales: Hammer is 32 cm long, coin is 1.9 cm diameter.

Figure 6: Summary depositional model for the supra-olistostrome interval. Following a glacial minimum (A), when the olistostrome was emplaced, ice sheets repopulated highlands. Uplands were a source area for both the olistostrome and supra-olistostrome gravity flow deposits. During glacial re-advance (B), icebergs delivered debris-laden material to the ice front. A fairly constant meltwater supply was maintained to generate repetitively stacked gravity flow deposits, and icebergs shed IRD. (C) Dynamic oscillation of the grounding line in the hinterland, in this case minor recession and cessation of iceberg calving, halted the delivery of IRD. Meanwhile, gravity flows continued to deliver sediment to the basin.

Figure 7: Gross depositional environments (palaeogeographic) sketch map of the Death Valley area during Kingston Peak times, showing the posited location of the ice front over Sperry Wash (see Busfield and Le Heron, this volume), with the southern Kingston Range representing a comparatively ice-distal location. The southern Kingston Range received thick

accumulations of turbidites and, less commonly, debrites ultimately derived from the ice margin located toward the NW.

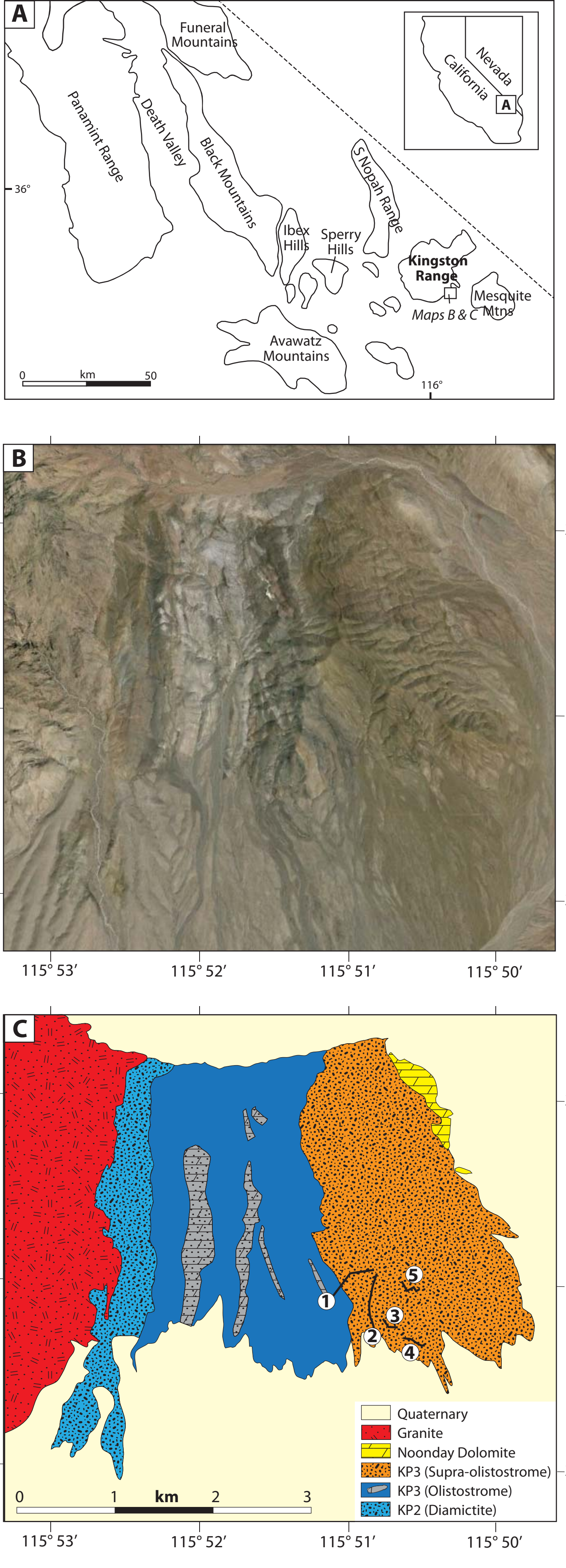
A
Funeral
Mountains
Panamint Range
Death Valley
Black Mountains
Nevada
California
A
36°
S Nopah Range
Ibex
Hills
Sperry
Hills
Kingston
Range
Mesquite
Mtns
Maps B & C
Avawatz
Mountains
0
km
50
116°
B
35° 43′
35° 42′
35° 41′
115° 53′
115° 52′
115° 51′
115° 50′
C
35° 43′
35° 42′
35° 41′
1
2
3
4
5
Quaternary
Granite
Noonday Dolomite
KP3 (Supra-olistostrome)
KP3 (Olistostrome)
KP2 (Diamictite)
0
1
km
2
3
115° 53′
115° 52′
115° 51′
115° 50′

Figure 1

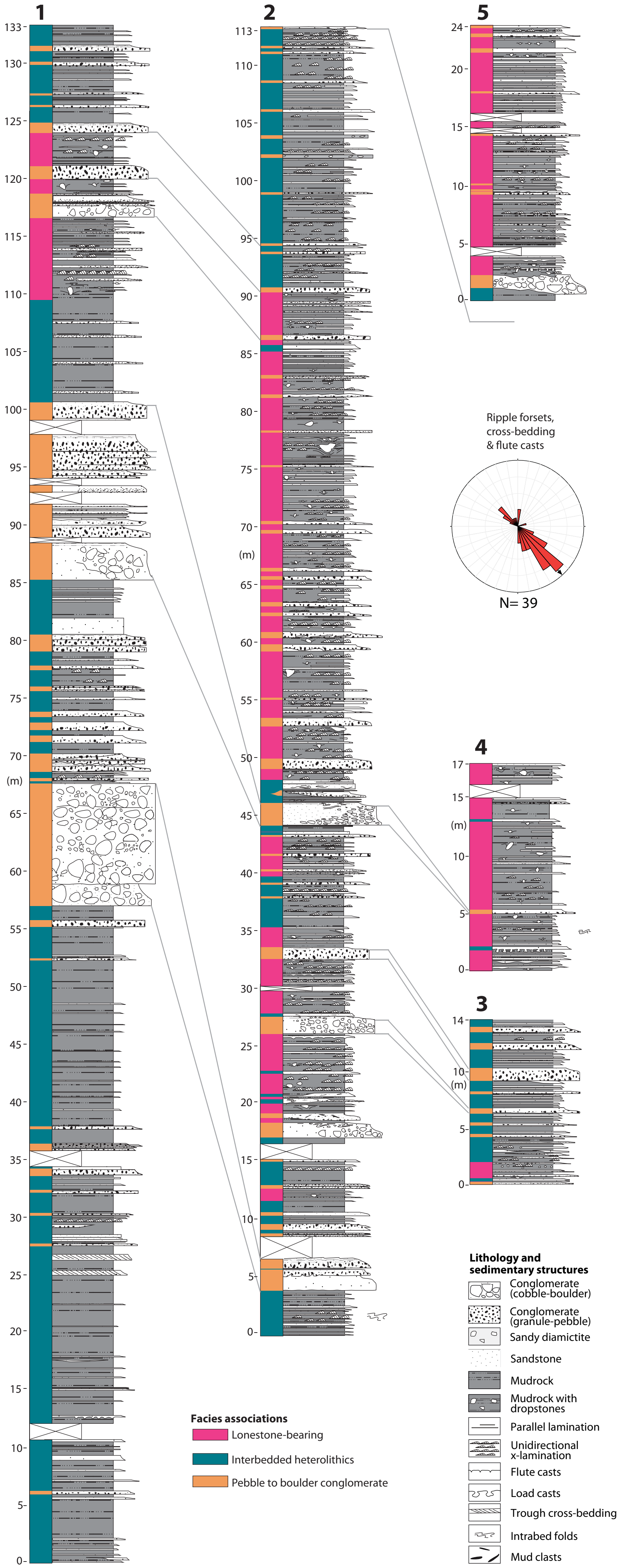

1
2
5
4
3
(m)
Ripple forsets, cross-bedding & flute casts
N= 39
Facies associations
Lonestone-bearing
Interbedded heterolithics
Pebble to boulder conglomerate
Lithology and sedimentary structures
Conglomerate (cobble-boulder)
Conglomerate (granule-pebble)
Sandy diamictite
Sandstone
Mudrock
Mudrock with dropstones
Parallel lamination
Unidirectional x-lamination
Flute casts
Load casts
Trough cross-bedding
Intrabed folds
Mud clasts

Figure 2

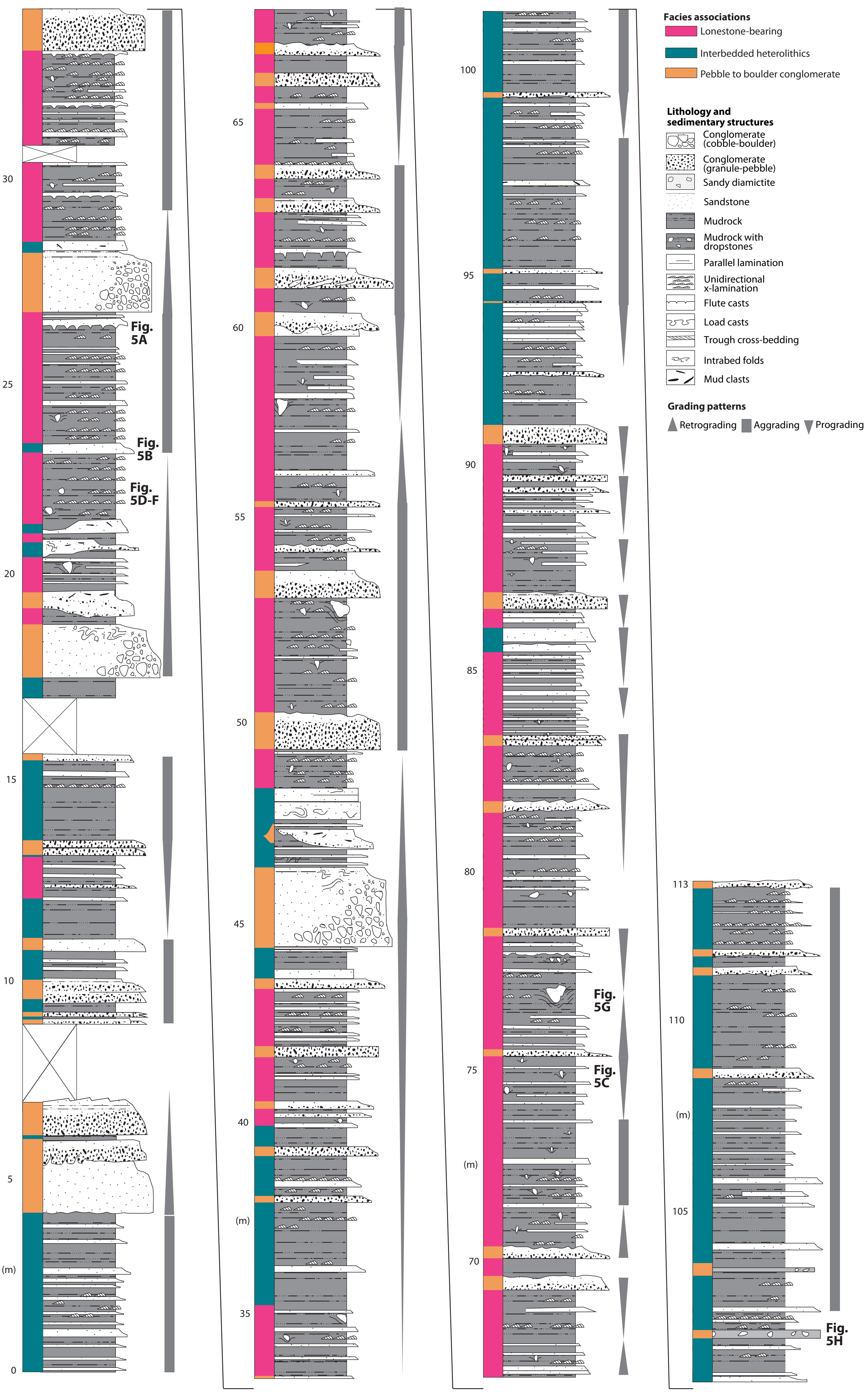

Facies associations
Lonestone-bearing
Interbedded heterolithics
Pebble to boulder conglomerate
Lithology and sedimentary structures
Conglomerate (cobble-boulder)
Conglomerate (granule-pebble)
Sandy diamictite
Sandstone
Mudrock
Mudrock with dropstones
Parallel lamination
Unidirectional x-lamination
Flute casts
Load casts
Trough cross-bedding
Intrabed folds
Mud clasts
Grading patterns
Retrograding
Aggrading
Prograding
Fig. 5A
Fig. 5B
Fig. 5D-F
Fig. 5G
Fig. 5C
Fig. 5H
(m)
0
5
10
15
20
25
30
35
40
45
50
55
60
65
70
75
80
85
90
95
100
105
110
113

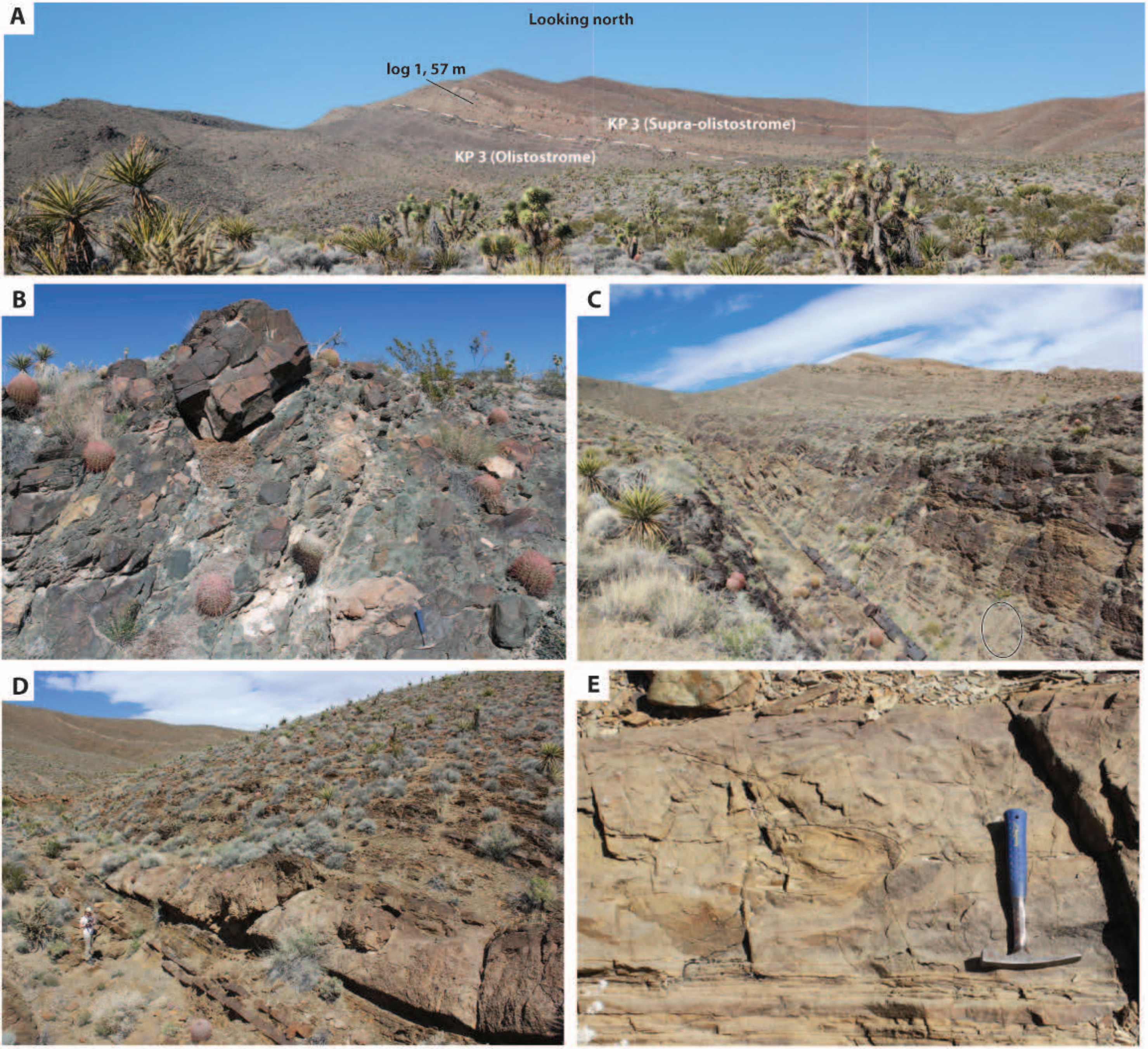
A
Looking north
log 1, 57 m
KP 3 (Supra-olistostrome)
KP 3 (Olistostrome)
B
C
D
E

Figure 4

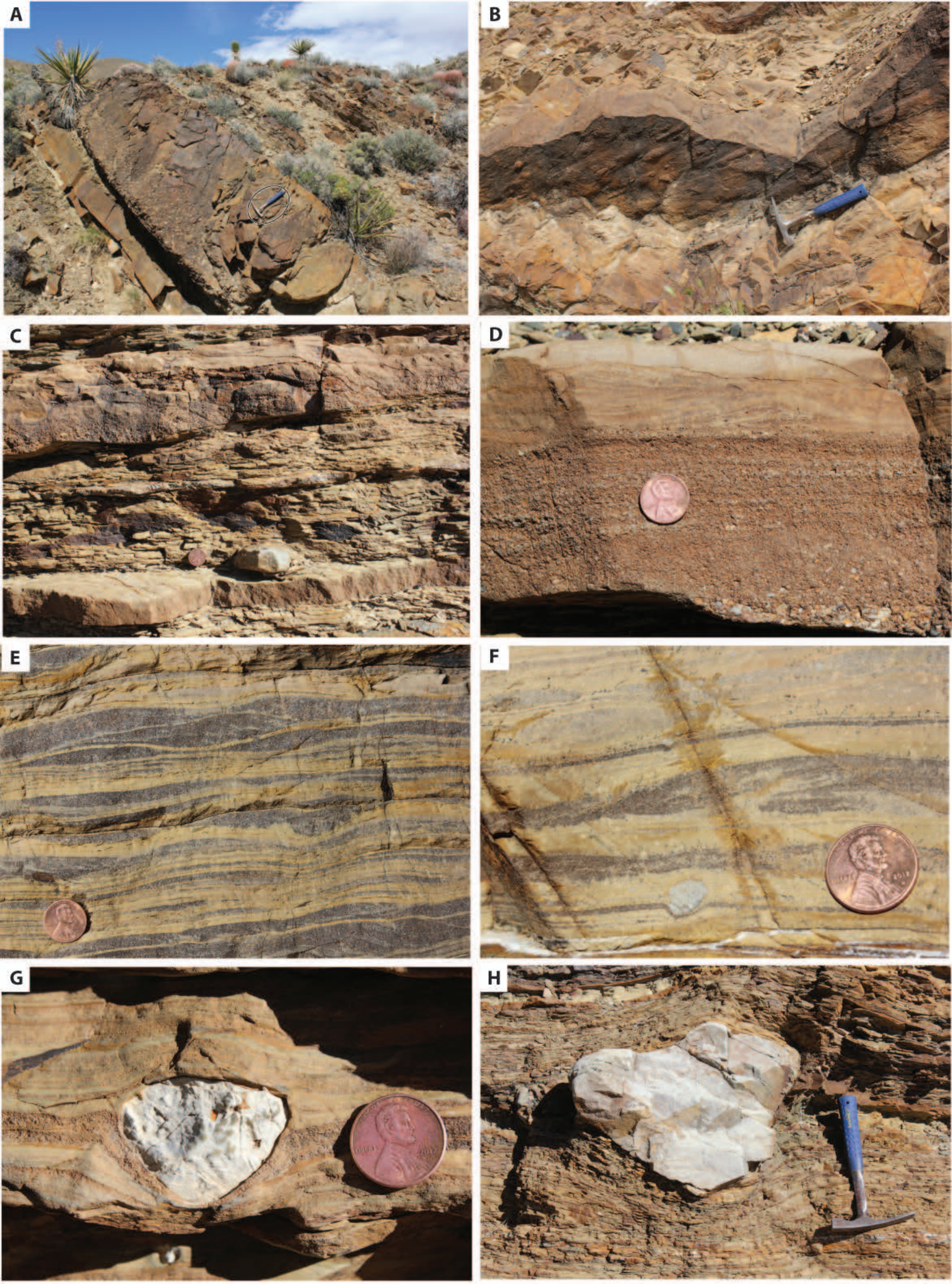

Figure 5

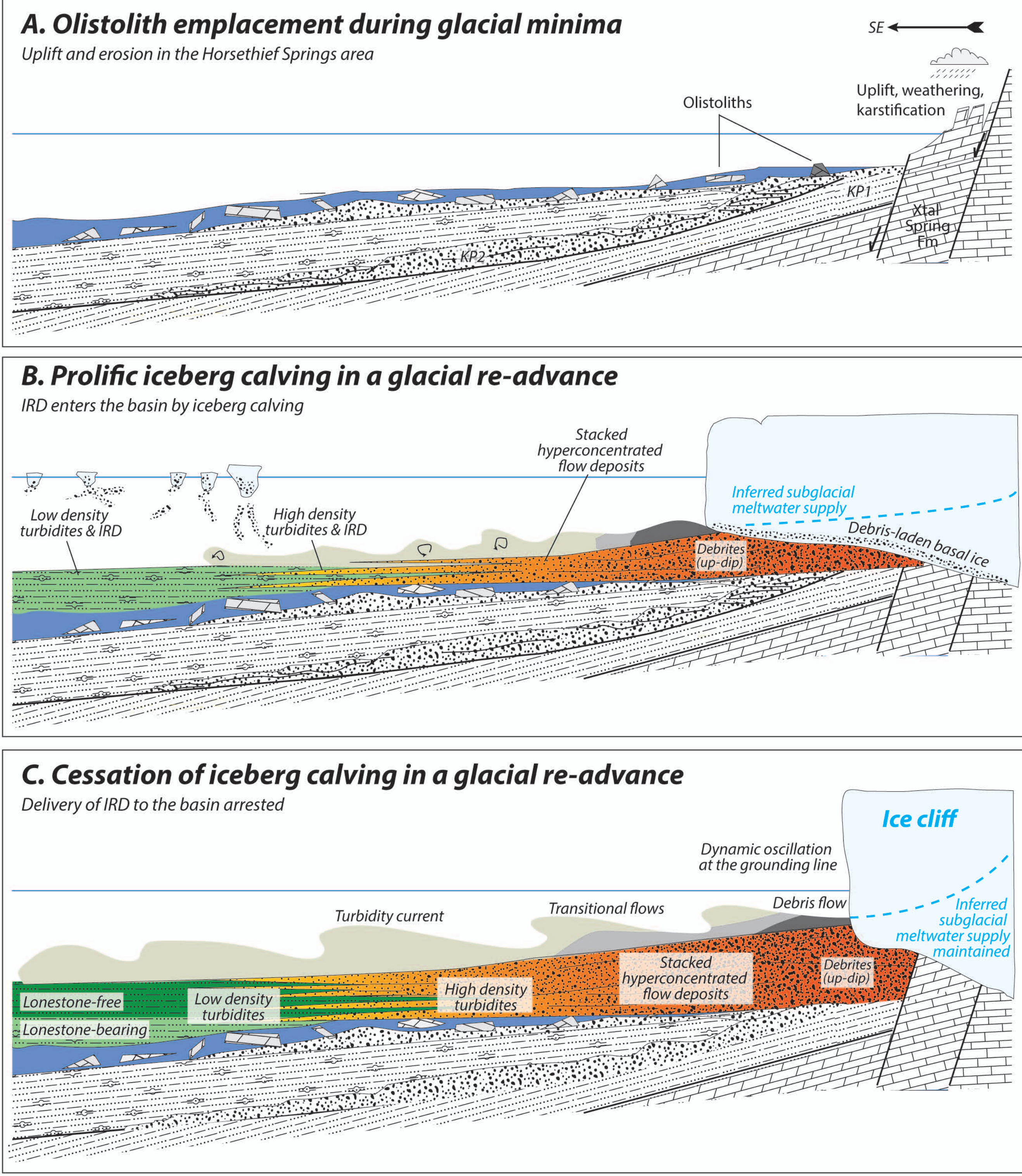

A. Olistolith emplacement during glacial minima
Uplift and erosion in the Horsethief Springs area
SE
Olistoliths
Uplift, weathering,
karstification
KP1
KP2
Xtal
Spring
Fm
B. Prolific iceberg calving in a glacial re-advance
IRD enters the basin by iceberg calving
Stacked
hyperconcentrated
flow deposits
Inferred subglacial
meltwater supply
Low density
turbidites & IRD
High density
turbidites & IRD
Debris-laden basal ice
Debrites
(up-dip)
C. Cessation of iceberg calving in a glacial re-advance
Delivery of IRD to the basin arrested
Ice cliff
Dynamic oscillation
at the grounding line
Debris flow
Transitional flows
Turbidity current
Inferred
subglacial
meltwater supply
maintained
Stacked
hyperconcentrated
flow deposits
Debrites
(up-dip)
High density
turbidites
Low density
turbidites
Lonestone-free
Lonestone-bearing

Figure 6

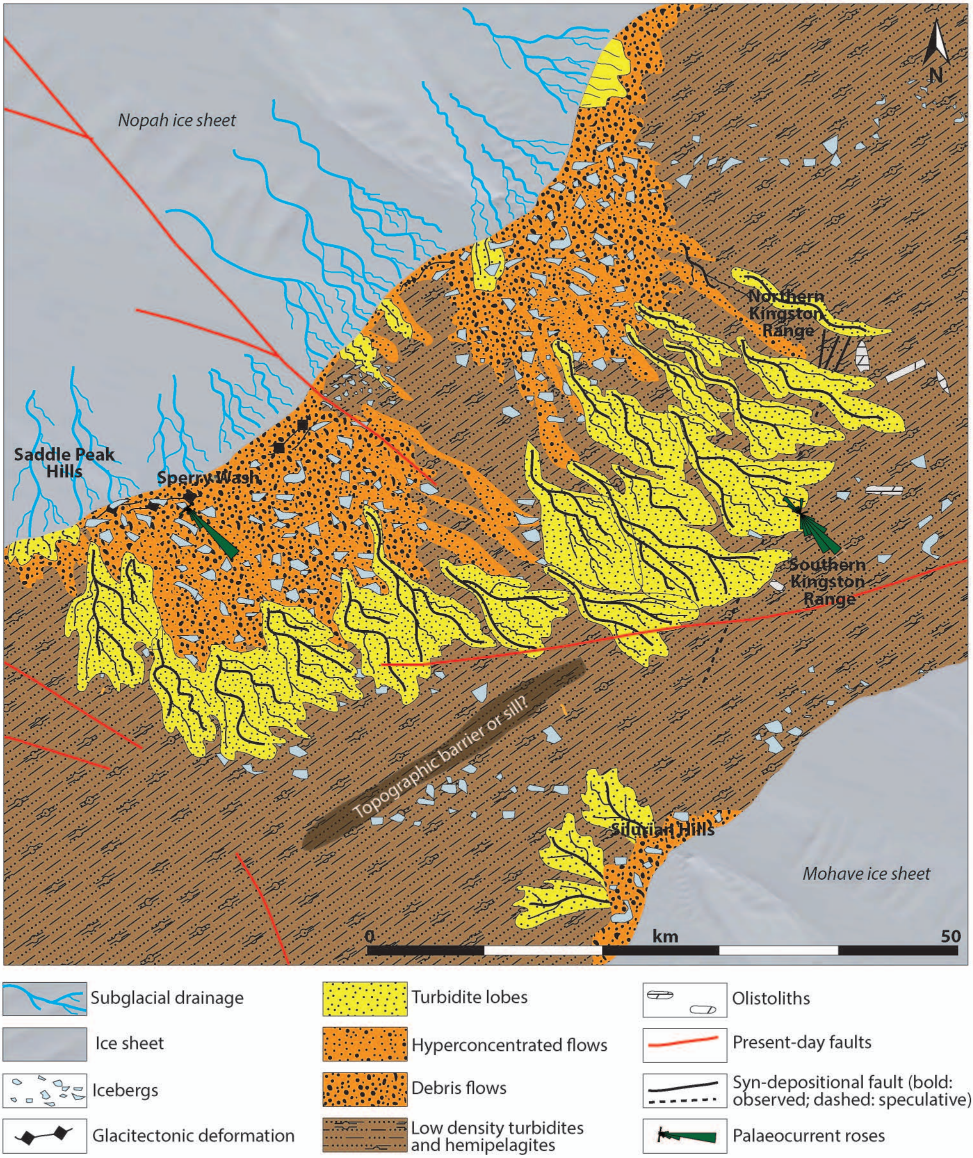
N
Nopah ice sheet
Saddle Peak Hills
Sperry Wash
Northern Kingston Range
Southern Kingston Range
Topographic barrier or sill?
Silurian Hills
Mohave ice sheet
0
km
50
Subglacial drainage
Ice sheet
Icebergs
Glacitectonic deformation
Turbidite lobes
Hyperconcentrated flows
Debris flows
Low density turbidites and hemipelagites
Olistoliths
Present-day faults
Syn-depositional fault (bold: observed; dashed: speculative)
Palaeocurrent roses

Figure 7